Extreme polar cap density enhancements along magnetic field lines during an intense geomagnetic storm

J.-N. Tu,[1] M. Dhar,[1] P. Song,[1] B. W. Reinisch,[1] J. L. Green,[2] R. F. Benson,[2] and A. J. Coster[3]

Received 21 August 2006; revised 12 November 2006; accepted 20 December 2006; published 2 May 2007.

[1] Sounding measurements from the radio plasma imager (RPI) on the IMAGE satellite are used to derive electron number density distributions along magnetic field lines in the polar cap magnetosphere during an intense magnetic storm. It is shown that electron densities along magnetic field lines in the polar cap magnetosphere were greatly enhanced on both the dayside and nightside during the storm, compared to the electron density profiles measured during periods of lower geomagnetic activities. The electron density enhancements were observed extending to 7 Earth radii (R_E) in altitude on the dayside, with the electron density value reaching about 10 cm^{-3} at 7 R_E altitude. The observed density enhancements were likely due to the enhanced cleft ion fountain during the storm although some of nightside density enhancements might be caused by the increased ion outflows locally in the polar cap. The strongest electron density enhancements observed on the dayside are possibly further associated with storm-time transport of plasma from the midlatitude ionosphere and plasmasphere to high latitudes, which manifests as a plasma plume intruding to dayside high latitudes as seen from total electron content (TEC) maps. With an enhanced source population supplied by the plasma plume, acceleration and heating processes in the dayside cusp/auroral region may produce a large flux of outflowing plasma along magnetic field lines while the outflowing plasma is convected anti-sunward toward the polar cap. These processes lead to strongly enhanced cleft ion fountain and thus greatly raised electron densities at magnetospheric altitudes in the polar cap. The present study captures an event of a massive redistribution of the magnetospheric and ionospheric plasma during a geomagnetic storm caused by extreme solar wind/interplanetary magnetic field (IMF) conditions.

Citation: Tu, J.-N., M. Dhar, P. Song, B. W. Reinisch, J. L. Green, R. F. Benson, and A. J. Coster (2007), Extreme polar cap density enhancements along magnetic field lines during an intense geomagnetic storm, *J. Geophys. Res.*, *112*, A05201, doi:10.1029/2006JA012034.

1. Introduction

[2] The polar ionosphere is regarded as a major source of plasma from the ionosphere to the magnetosphere through the pervasive polar wind (primarily hydrogen ions H^+) and intermittent heavy ions (primarily oxygen ions O^+) outflows at least during geomagnetically active times [e.g., *Moore and Delcourt*, 1995; *Chappell et al.*, 2000] Although still controversial, *Chappell et al.* [1987] concluded that the ionosphere alone was able to supply the entire plasma content of the magnetosphere under all geomagnetic conditions by estimating volumes and ion residence times for the plasmasphere, plasma trough, plasma sheet, and magnetotail lobes. Thermal plasma of ionospheric origin has been observed, at one time or another, nearly everywhere in the magnetosphere from in situ observations. Therefore the study of extreme plasma density enhancements in the polar cap is of considerable interest.

[3] Plasma densities in the polar cap ionosphere and magnetosphere are highly variable and structured because of complex chemical and dynamic processes. For example, localized electron density (N_e) enhancements (polar patches) can form at ionospheric F-layer altitudes when the midlatitude ionosphere plasma is transported across the dayside cusp into the polar cap by time varying plasma convection [e.g., *Whitteker et al.* 1976; *Rodger et al.* 1994; *Sojka et al.* 2006]. The O^+ density trough (with density as low as 0.01 cm^{-3}) at about 1 Earth radius (R_E) in altitude is observed on the nightside polar cap when there is a lack of source O^+ in the ionospheric F-layer [*Zeng et al.* 2004]. The plasma density at polar magnetosphere altitudes can be

[1]Center for Atmospheric Research, University of Massachusetts Lowell, Massachusetts, USA.
[2]NASA Goddard Space Flight Center, Greenbelt, Maryland, USA.
[3]MIT Haystack Observatory, Westford, Massachusetts, USA.

Copyright 2007 by the American Geophysical Union.
0148-0227/07/2006JA012034

increased by the enhanced cleft ion fountain or the increased ion outflows locally in the polar cap ionosphere [*Horwitz and Moore*, 1997; *Schunk and Sojka*, 1997; *Schunk*, 2000; *Tu et al.*, 2004].

[4] In the dayside cusp/auroral region the heating/acceleration processes cause ionospheric ion outflows along the magnetic field lines and outflowing ions are meanwhile transported to the polar magnetosphere by the anti-sunward convection. The heating/acceleration processes and anti-sunward convection together were termed as cleft ion fountain, which can supply plasma to the polar magnetosphere [*Horwitz*, 1984; *Lockwood et al.* 1985; *Tsunoda et al.*, 1989; *André et al.*, 1990; *Horwitz and Moore*, 1997; *Moore et al.*, 1999; *Dubouloz et al.*, 2001; *Tu et al.*, 2005a]. The cleft ion fountain can be enhanced by the increased energy input (through increased Poynting flux and soft-electron precipitation flux) to the polar ionosphere at times of geomagnetic disturbances. This is because the increased energy input increases both the effects of the heating/acceleration processes and the ionospheric ion (primarily O^+) density in the heating/acceleration region that provides an augmented source population for the ion outflows.

[5] The cleft ion fountain may be even more strongly increased during major magnetic storms when there is a large flux of midlatitude ionospheric plasma transporting to the dayside cusp/auroral region. During the major magnetic storms, the dayside midlatitude ionospheric density can be enhanced by the uplift of the low-latitude F-layer plasma and the diffusion of the lifted plasma along magnetic field lines to higher latitudes [e.g., *Warren*, 1969; *Evans*, 1973; *Tanaka*, 1979; *Foster*, 1993; *Buonsanto*, 1999; *Tsurutani et al.*, 2004; *Huang et al.* 2005]. Rapid poleward convection then carries a large flux of midlatitude ionospheric plasma through the dayside cusp into the polar cap as the feet of the flux tubes move from the middle latitudes to the higher latitudes [e.g., *Pryse et al.*, 2004; *Foster et al.*, 2005]. Meanwhile, the plasmaspheric plasma in the outer region of the plasmasphere (close to the plasmapause) is stripped away and transported to the dayside magnetopause by subauroral polarization stream (SAPS)-associated sunward convection, which is seen as a plasmaspheric drainage plume from extreme ultraviolet (EUV) images taken by the IMAGE satellite [e.g., *Burch et al.*, 2001]. The plasmaspheric drainage plume and the midlatitude ionospheric plasma transported to high latitudes have recently been observed to occur along common flux tubes extending from the ionosphere to the plasmasphere [*Garcia et al.*, 2003; *Foster et al.*, 2002, 2004]. A recent estimate made by *Foster et al.* [2004] using combined observations with a network of GPS total electron content (TEC) receivers, the Millstone Hill incoherent scatter radar, and DMSP and IMAGE satellites indicates a rate of plasma transported toward the cusp up to 10^{26} ions/s (primarily O^+) during a large geomagnetic disturbance. The transported plasma includes contribution from both the ionosphere and the plasmasphere. However, a major contribution to the transported plasma is believed to be from the ionosphere because of the much higher ionospheric density. Such a large rate of ionospheric plasma transporting to high latitudes provides a strongly increased source population for the potentially large flux of plasma outflow to the magnetosphere from the dayside cusp/auroral region [*Foster et al.*, 2005], i.e., strongly enhanced cleft ion fountain. It is expected that the plasma density in the polar cap magnetosphere be raised through the strongly enhanced cleft ion fountain. Assuming that this mechanism generates density enhancements, questions arise such as how strong and up to what altitude these density enhancements can be observed. The answers to these questions are important because they may provide clues to the strength and altitude distribution of the heating/acceleration processes in the dayside cusp/auroral region.

[6] The purpose of this paper is to determine the electron density (N_e) profiles (up to 7 R_E altitude) along the geomagnetic field lines in the polar cap magnetosphere during the intense magnetic storm which occurred on 31 March 2001, using measurements from the radio plasma imager (RPI) on the IMAGE satellite [*Burch et al.*, 2001]. Two active RPI sounding modes were in operation during this time period. One, using short (3.2 ms) pulses, had high-frequency resolution (300 Hz) and was designed for accurate detection of plasma resonances; and the other, using two long (51.2 ms) phase-coded pulses, employed coherent integration to improve the signal-to-noise ratio so as to detect long-range echoes [*Reinisch et al.*, 2000]. *Osherovich et al.* [2001, 2007] and *Benson et al.* [2003, 2006] used the former to detect in situ increases in the electron plasma frequency f_{pe} (and thus N_e) and the electron cyclotron frequency f_{ce} (and thus the magnetic field B) near 7 R_E altitude, while here we use the latter to show that field-aligned N_e profiles, extending from $\sim$4 R_E to $\sim$7 R_E altitude, are strongly enhanced. The measured field-aligned N_e profiles during the storm are nearly two orders of magnitude higher than the normally observed and even consistently higher when compared to empirical N_e models of the polar cap during times of high geomagnetic activity. The field-aligned N_e profiles are inverted from distinct echo traces on the plasmagrams recorded by the IMAGE RPI. Because of typically very low density at IMAGE apogee ($\sim$7 R_E altitude) in the polar cap, the local plasma frequency is below the lower frequency limit (3 kHz) of those sounding programs that corresponds to an electron density of less than 0.1 cm^{-3}. Under normal conditions, it is rarely possible to measure complete field-aligned N_e profiles at altitudes above $\sim$4 R_E, although there are a large number of field-aligned N_e profiles measured below that altitude in the polar cap [*Nsumei et al.*, 2003; *Tu et al.*, 2005b].

[7] To examine possible mechanisms of the observed polar magnetospheric density enhancements, we also examine global maps of the vertical total electron content (TEC) derived from a network of global positioning system (GPS) receivers, DMSP satellite measurements of topside ionosphere ion densities and velocities in the polar cap, as well as electron densities and velocities measured in the polar cap F-region by a Digisonde. In section 2, we briefly describe the RPI measurement technique and geophysical conditions on 31 March 2001. The observed N_e enhancements are presented in section 3, followed by the observations of GPS TEC in section 4, and ionospheric plasma

Table 1. UT, Radial Distance r (R_E), Invariant Latitude (ILAT) of the IMAGE RPI Measurements on 31 March 2001[a]

Group 1: Nightside					
	UT	r	ILAT, deg	MLAT, deg	MLT
1	1419	4.64	67.3	69.9	2329:58
2	1425	4.79	68.1	70.8	2330:08
3	1437	5.08	69.3	72.2	2327:47
4	1443	5.22	70.2	73.1	2326:21
5	1513	5.83	74.4	77.4	2320:45
6	1525	6.06	76.5	79.4	2320:04
Group 2: Dayside					
	UT	r	ILAT, deg	MLAT, deg	MLT
1	1838	8.01	82.3	82.8	1109:16
2	1942	8.10	78.0	78.7	1108:24
3	1948	8.10	77.8	78.3	1107:36
4	2006	8.07	76.8	77.5	1106:12
5[b]	2130	7.68	76.4	77.1	1107:48

[a]Also listed are the magnetic latitude (MLAT) and magnetic local time (MLT) of the satellite footprint. The footprint is obtained by projecting the IMAGE Orbit to 300 km altitude along the magnetic field lines calculated with the T01 Magnetic Field Model [*Tsyganenko*, 2002].

[b]TEC plume existed at magnetic latitudes below 60°.

velocity and density in section 5. The discussion and summary are given in section 6.

2. IMAGE RPI Measurement Technique and Geophysical Conditions

[8] The RPI instrument alternated between making passive radio wave measurements and radio sounding measurements. Each of these modes of operation is analyzed and displayed differently. The design and measurement characteristics of the IMAGE RPI have been described in detail by *Reinisch et al.* [2000] and the inversion technique used to derive field-aligned N_e profiles has been discussed in previous studies [*Reinisch et al.*, 2001, 2004; *Huang et al.*, 2004; *Song et al.*, 2004]. In brief, the RPI, in active sounding modes, transmitted coded signals stepping through frequencies from 3 kHz to 3 MHz and detected the echoes. The received echoes are plotted in a "plasmagram" with the analysis software known as BinBrowser [*Galkin et al.*, 2004]. A plasmagram is a color-coded display of signal amplitude as a function of frequency and echo delay time (represented as virtual range: one-half of the echo delay time multiplied by the speed of light in free space). Multifrequency echoes can form distinct traces in a plasmagram. It has been found that when discrete traces are observed they correspond to reflected signals that propagate along the magnetic field line threading the satellite [*Reinisch et al.*, 2001; *Fung et al.*, 2003; *Fung and Green*, 2005]. Applying a new inversion algorithm [*Huang et al.*, 2004], we can derive the N_e distribution along a field line almost instantaneously (in $\leq$ 1 min). The transmitted signals also stimulate local (at satellite locations) plasma resonances that can be used to determine the in situ electron cyclotron harmonic frequencies and plasma frequency [*Benson et al.*, 2003].

[9] The magnetic storm on 31 March 2001 was an intense storm with the hourly Dst index decreasing to $\sim$−387 nT. After the storm started at about 0600 UT on 31 March 2001, Dst decreased dramatically and reached its minimum at about 0900 UT. During the short (about 3 hours) main phase of the storm, IMAGE crossed the dayside polar cap from its apogee (about 7 R_E altitude) in the central polar cap to lower latitudes on the dayside. Along this orbit segment, IMAGE RPI did not record any plasmagrams that show traces in the polar cap although a number of plasmagrams with clear traces were measured in the plasmasphere [*Reinisch et al.*, 2004]. A possible reason is that the electron density in the polar cap, at least along the IMAGE orbit, had not elevated to the level that allowed the echo traces to be detectable with the RPI sounder programs in operation. It is also likely that the strong disturbances during the storm main phase do not favor the guided propagation of the signals. Nevertheless, during the storm recovery phase, along a subsequent polar cap pass the IMAGE RPI recorded a number of plasmagrams containing traces that can be used to derive field-aligned N_e distributions in the polar cap. Table 1 lists times and locations of these measurements, which were made along a single IMAGE pass across the northern polar cap from nightside to dayside.

[10] The top panel of Figure 1 shows the variation of the hourly Dst index from 1200 UT on 30 March 2001 to 0000 UT

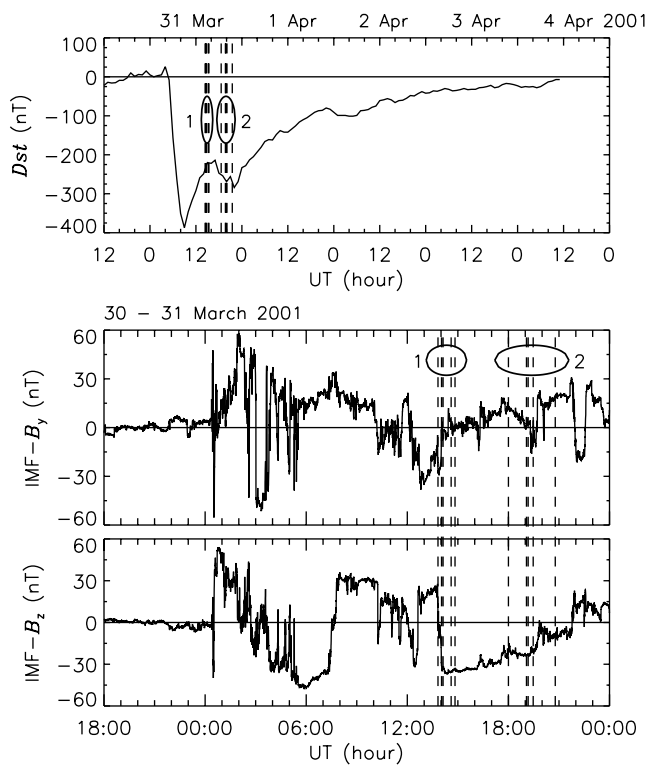

Figure 1. Top panel is Dst index from 1200 UT on 30 March 2001 to 0000 UT on 5 April 2001. The bottom two panels are IMF B_y and B_z, respectively, measured by ACE spacecraft at $X_{GSM} = \sim 223\ R_E$ on 31 March 2001. The vertical dashed lines on the Dst panel indicate the times of IMAGE RPI measurements listed in Table 1. Dashed vertical lines on the IMF panels indicate roughly the times of the solar wind/IMF measurements by the ACE corresponding to the RPI measurements. The vertical lines on IMF panels have been backward-shifted to account for the solar wind transition time from the ACE location to the magnetopause. Measurements marked by ovals 1 and 2 are made on the nightside and dayside, respectively.

on 5 April 2001. The vertical dashed lines indicate the times of the IMAGE RPI plasmagram measurements. The vertical lines are organized into two groups and each is marked by an oval: group 1 represents the measurements made on the nightside and group 2 on the dayside as indicated by magnetic local time (MLT) listed in Table 1. The vertical lines for group 1 are barely differentiable because the measurement times are close to each other. It is noted that group 2 measurements were made during a decrease of the Dst index with Dst ~ -260 nT in the storm recovery phase. This Dst decrease was driven by a period of persistently negative interplanetary magnetic field (IMF) B_z as noted from the IMF B_z panel of Figure 1. The vertical dashed lines on the IMF panels are approximately corresponding times of the Advance Composition Explorer (ACE) spacecraft measurements in the upstream solar wind. The solar wind transition time from the ACE location to the magnetopause was taken into account when drawing the vertical lines on the IMF panels. It is seen that the nightside measurements were carried out around IMF B_z reorientation from northward to southward and IMF B_y was generally negative. The dayside measurements were made in a period of persistently southward IMF with IMF $B_z = -20$ nT. The IMF B_y during the period of dayside measurements was positive. Among 5 dayside measurements, measurements 1–4 were made within the period of a TEC plume extending to above 65° (up to 70°) magnetic latitude (MLAT), but measurement 5 was obtained after the TEC plume had retreated to latitudes below 60°, as will be shown later by the GPS TEC maps.

3. Polar Cap Density Enhancements

[11] In this section, we present observations of the field-aligned N_e profiles measured by the IMAGE RPI in the polar cap. As mentioned previously, the sounding measurement programs of the RPI that captured traces during the 31 March 2001 storm used long transmitter pulses (51.2 ms). Such long transmitter pulses prevented some short-duration (low virtual range on the plasmagrams) resonances from being detected, making it more difficult to determine f_{ce} and f_{pe} at the satellite. This difficulty can be overcome, however, by first identifying some of the stronger resonances at the nf_{ce} harmonics, with the aid of a model for the magnetic field B, so as to determining f_{ce} at the satellite. Using this f_{ce} value, the ambient f_{pe} value is obtained from a self-consistent identification of the sounder-stimulated resonances at f_{pe} and at the upper hybrid frequency f_{uh} ($f_{uh}^2 = f_{pe}^2 + f_{ce}^2$), as well as the projection of the X-mode trace to its cutoff value f_x at the satellite given by $f_x = (f_{ce}/2)\,[1 + (1 + 4f_{pe}^2/f_{ce}^2)]^{1/2}$.

[12] An additional aid in the self-consistent identification of the above features is provided by two series of resonances often observed between the nf_{ce} harmonics. One series, known as the Qn resonances, are observed at frequencies greater than f_{uh} and are due to sounder-stimulated electrostatic Bernstein-mode waves with group velocity comparable to the satellite velocity [*Muldrew*, 1972]. The other, known as the Dn resonances, are observed at frequencies less than f_{pe} and have been explained in terms of sounder-stimulated electromagnetic cylindrical plasma oscillations as described in the review by *Osherovich et al.* [2005]. The frequencies of the resonances in both of these series are dependent mainly on the ratio f_{pe}/f_{ce}, so they provide an extra degree of confidence in the identification of the proper features as f_{pe} and f_{uh} on RPI plasmagrams, particularly when f_x is present, as described by *Benson et al.* [2003]. The accuracy of the ambient f_{ce} and f_{pe} determinations is dependent on the frequency resolution of the RPI sounding mode in use. This resolution is typically a few percent for the modes used for long-range sounding. Thus the ambient f_{ce} and f_{pe} can be determined to this accuracy. The accuracy of the ambient N_e is less but is typically better than 10%. The remote N_e profile along the magnetic field direction is obtained by inverting the X-mode virtual range/frequency trace; confidence in this approach is obtained by using the resulting N_e profile to correctly calculate the virtual range/frequency traces of other independent modes of propagation when they are observed [*Huang et al.*, 2004]. Tests of the accuracy of such N_e profiles have been performed in the topside ionosphere. For example, conjunction comparisons between Langmuir-probe measurements on the low-altitude Dynamics Explorer-2 satellite and topside-sounder measurements on the higher-altitude International Satellites for Ionospheric Studies (ISIS1 and ISIS2) demonstrated the good accuracy of the topside N_e profiles at all altitudes from the satellite down to the F-region peak density (where the agreement was typically about 30%) [*Hoegy and Benson*, 1988].

3.1. Density Enhancements on the Nightside

[13] During the IMAGE nightside polar cap pass from 1400 to 1530 UT on 31 March 2001, the RPI recorded a number of plasmagrams with operation Program 59 which used long transmitter pulses. Among those plasmagrams, six contain a clear X-mode trace from which we can derive a field-aligned N_e profile. These six plasmagrams were obtained at radial distances below 6.0 R_E. One of these plasmagrams, recorded at 1443 UT with Program 59, is displayed in Figure 2. Local (at the satellite location) plasma resonances (vertical lines with enhanced signal strength) are identified on the plasmagrams. The electron cyclotron harmonics are indicated by red arrows at the top of the plasmagram and are also labeled with numbers at the bottom. The symbols P, U, and X represent the electron plasma resonance, the upper hybrid resonance, and the X-mode wave cutoff, respectively. On the plasmagram shown in Figure 2, the $2f_{ce}$ and $4f_{ce}$ resonances are the most definite electron cyclotron harmonic resonances. From the values of $2f_{ce}$ and $4f_{ce}$ we get f_{ce} = 13.66 kHz. Because of the short duration of the higher harmonic resonances and the long transmitter pulses, the $5f_{ce}$ and $6f_{ce}$ harmonic resonances on the plasmagram are not prominent. Note that the virtual range scan of Program 59 starts from 1.2 R_E. The $5f_{ce}$ and $6f_{ce}$ harmonic resonances may have virtual ranges below 1.2 R_E so they are not visible on the plasmagram. The identification of the f_{pe} or f_{uh} resonance is constrained by the variation trend of the X-mode trace. A feature of the X-mode wave propagation near the cutoff frequency f_x is that the projection of the X-mode trace on the plasmagram to f_x at zero virtual range must give a very steep gradient to the trace in virtual range [e.g., *Stix*, 1962]. Because of this requirement, along with a resonance at 30.2 kHz on the Z-antenna signal which we identify as f_{uh} (not clearly seen in Figure 2), we have no other choice but to locate the f_{pe} resonance at a frequency of 26.93 kHz, which is indicated

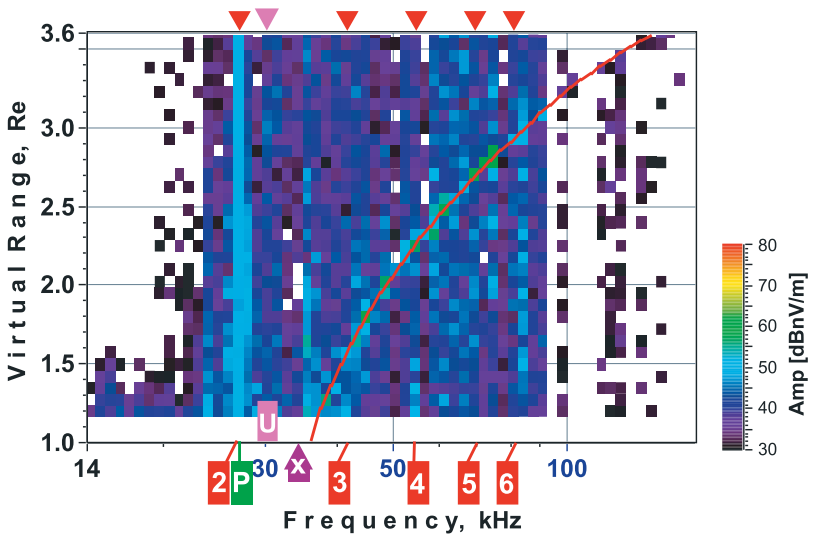

Figure 2. A plasmagram recorded at 1443 UT on 31 March 2001. The electron cyclotron harmonic resonances are marked by red arrows at the top and are also labeled with numbers at the bottom. Symbols P, U, and X are electron plasma frequency, upper hybrid frequency, and X-mode cutoff frequency, respectively. The values of f_{ce}, f_{pe}, f_{uh}, and f_x are 13.66, 26.93, 30.2, and 34.62 kHz, respectively. An X-mode trace extends from about 38.5 to 140.8 kHz.

by a symbol P and, in combination with the resonance at $2f_{ce}$, appears as the most definite resonant feature on the plasmagram. The local N_e is calculated from the relation $f_{pe} \approx [80.6N_e\ (\mathrm{cm}^{-3})]^{1/2}$ to be 8.9 cm^{-3}. The X-mode cutoff is then determined to be at f_x = 34.62 kHz.

[14] After scaling the X-mode trace (thin red line), which extends from about 38.5 to 140.8 kHz, we derive a field-aligned N_e profile using the algorithm described by *Huang et al.* [2004]. As mentioned previously, the values of f_{ce} and f_{pe} can be determined to the accuracy of the frequency resolution of the sounding programs in use. In Program 59 the largest frequency step below 60 kHz, where $2-4f_{ce}$ and f_{pe} are detected, is near 2.3 kHz. Using upper and lower limits for f_{ce} and f_{pe} based on minus and plus one half of this amount, we project the X-mode trace to zero virtual range at different f_x values on the plasmagram shown in Figure 2 and then perform the electron density inversion for each of those scaled traces. This procedure provides an estimate of the uncertainty in the inverted density profile. The uncertainty is estimated to be up to 20% for the density profiles inverted from the traces on the six plasmagrams mentioned above.

[15] The above procedure for identifying f_{ce} and f_{pe} and scaling the trace is applied to six plasmagrams recorded on the nightside. The N_e profiles derived from the traces on the six plasmagrams are displayed in Figure 3. We also show the average N_e profiles for the altitude range of 3000 km to ~4 R_E from an empirical model of the polar cap electron density [*Nsumei et al.*, 2003] for 3-hour index Kp = 3 (dashed line) and Kp = 8 (dotted line). Kp = 8 is the highest Kp value in the data set of *Nsumei et al.* [2003]. As shown in Figure 3, during this magnetic storm, the nightside polar magnetosphere densities up to 5 R_E altitude are enhanced to a level higher than the densities given by the model of Nsumei et al. for Kp = 8. Figure 3 also shows that the enhancement is larger with increasing altitude. At the bottom of each measured density profile, the electron density is approximately the same as that given by the empirical model at the same altitude for Kp = 8.

3.2. Density Enhancements on the Dayside

[16] On the dayside, the RPI recorded five plasmagrams with traces when IMAGE flew across its apogee toward lower latitudes from the central polar cap. Those five plasmagrams were recorded with operation Program 18, which receives signals with a frequency range of 20–74 kHz and samples virtual range up to 12.1 R_E. Program 18 also used long transmitted pulses (51.2 ms). In addition, the lowest frequency sampled on the Program 18 plasmagrams is about four times higher than the local f_{ce} along the satellite orbit (at about 7 R_E altitude). Therefore the determination of f_{ce} is aided by plasmagrams recorded with Program 38 at about 1–2 min earlier than each of those five plasmagrams. The swept frequency range of Program 38 is from 3 to 48 kHz (in 151 frequency steps with frequency step 0.3 kHz, sampling virtual range up to 4.2 R_E after each short transmission pulse of 3.2 ms). The local resonances, particularly the electron cyclotron harmonics nf_{ce}, can be accurately determined on the Program 38 plasmagrams [*Benson et al.*, 2003]. The f_{pe} values determined on those plasmagrams are also helpful in determining f_{pe} on the Program 18 plasmagrams.

[17] In Figures 4 and 5, we display two consecutively recorded plasmagrams: the first one obtained with Program 38 at 2129 UT and the second one measured with Program 18 at 2130 UT (measurement 5 of group 2). Only a portion of the plasmagram recorded at 2129 UT with frequency range from 6 to 48 kHz is displayed, since the range below 6 kHz does not provide useful sounding measurements for plasma resonances [see *Benson et al.*, 2003]. The f_{ce} harmonics from $2-9f_{ce}$ (indicated by numbers below and red arrows on top) accompanied by strong Qn (Q2–Q8) resonances (indicated by blue arrows on top), can be clearly seen on this plasmagram. In this example, Q2 and Q3 are

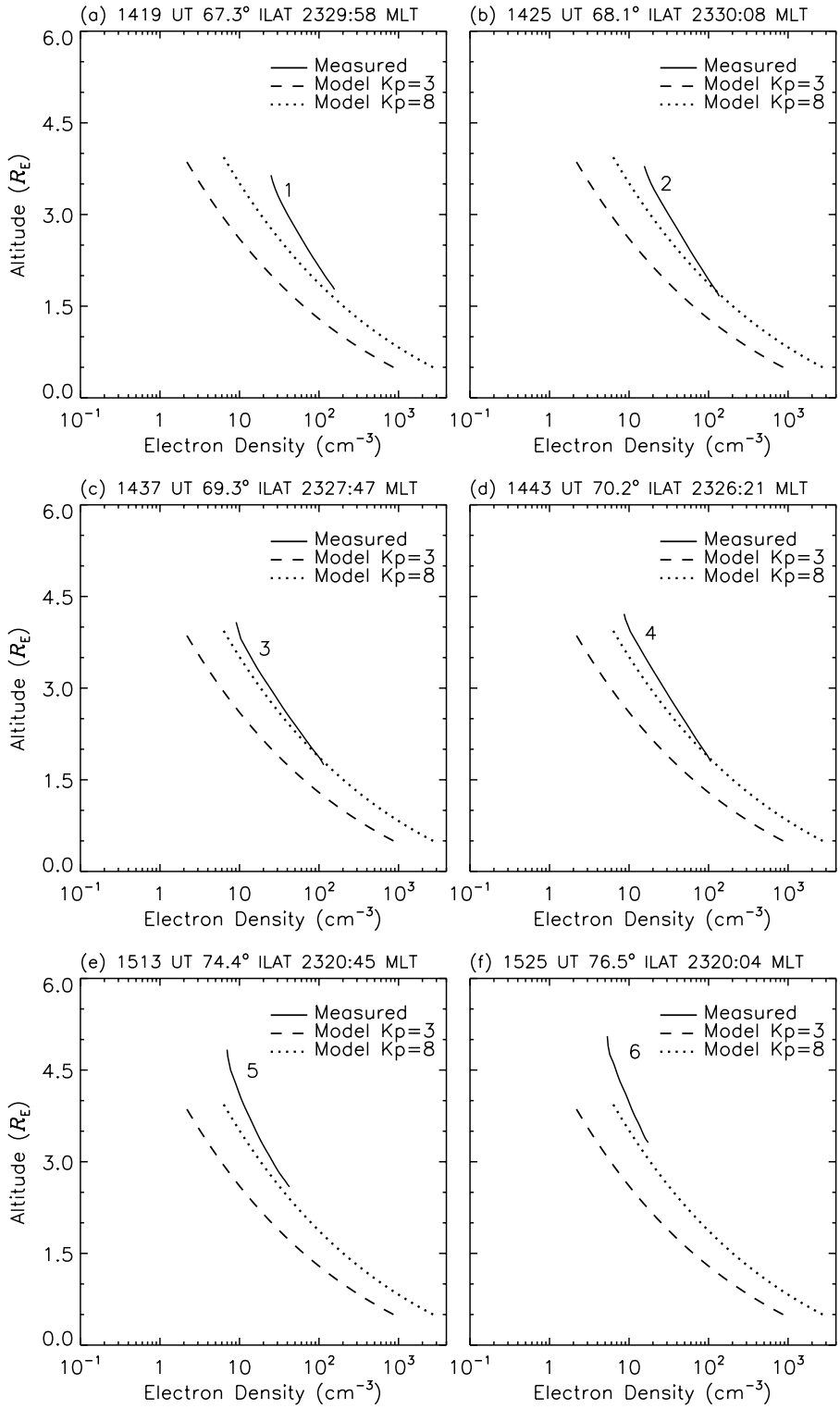

Figure 3. Field-aligned density profiles measured by the RPI in the nightside polar cap at the times listed in group 1 of Table 1. Panels (a)–(f) correspond to measurements 1–6. The dashed and dotted lines are density profiles from the empirical model of polar cap electron densities [*Nsumei et al.*, 2003] for Kp = 3 and Kp = 8, respectively.

well separated from (and at higher frequencies than) $2f_{ce}$ and $3f_{ce}$, respectively, but the higher Qn resonances merge with the nf_{ce} resonances. The f_{ce} value is determined either by using the nf_{ce} values near the f_{pe} and f_{uh} resonances or by using a model (or user input) value for the gradient of f_{ce} during the time interval of the plasmagram recording by taking into account the stepping time of sounding frequencies using the BinBrowser software [*Galkin et al.*, 2004].

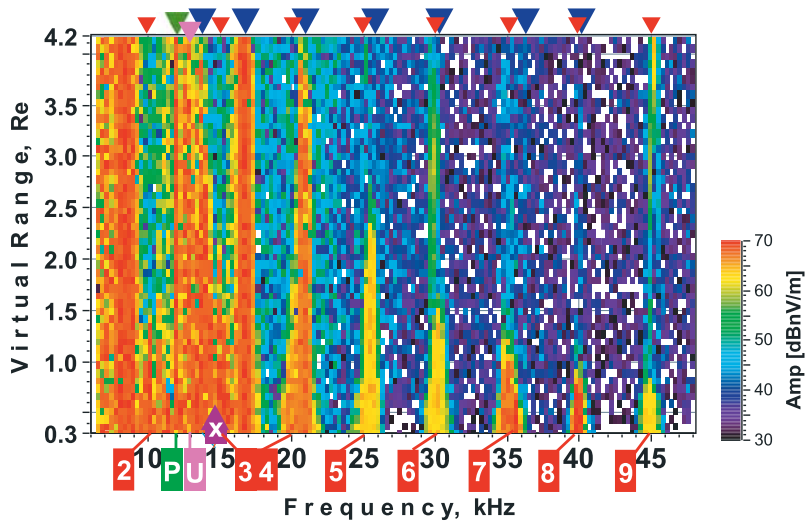

Figure 4. A plasmagram recorded with Program 38 at 2129 UT on 31 March 2001. The identified electron cyclotron harmonics $2-9f_{ce}$ are marked by arrows at the top and numbers at the bottom. Symbols P, U, and X are electron plasma frequency, upper hybrid frequency, and X-mode cutoff frequency, respectively. Blue arrows at the top indicate the Qn (Q2–Q8) resonances. The values of f_{ce}, f_{uh}, f_{pe}, and f_x are 5.0, 13.0, 12.0 and 14.76 kHz, respectively.

Using the former approach, with clearly resolved $2f_{ce}$ and $3f_{ce}$ resonances (i.e., no overlapping Qn resonances), the resultant value of f_{ce} is 5.0 kHz and the values of f_{uh}, f_{pe}, and f_x are 13.0, 12.0, and 14.76 kHz, respectively, the same as those determined by *Osherovich et al.* [2001, 2007] and *Benson et al.* [2006]. High-resolution plasmagrams of the type shown in Figure 4 can yield f_{pe} and f_{ce} values with uncertainties of the order of 1% and 0.1%, respectively [*Benson et al.*, 2003]. During the period of measurements, the IMAGE satellite was in the high-altitude polar cap. The value of f_{ce} should not change dramatically in about 1 min from 2129 to 2130 UT since the satellite did not cross any boundary layers with large magnetic variations, although the f_{ce} value may vary slightly as to be seen below.

[18] With the aid of the f_{ce} value from the plasmagram shown in Figure 4, we identify the 5th–11th electron cyclotron resonance harmonics on the plasmagram obtained with Program 18 at 2130 UT (Figure 5). Note again that some of the higher f_{ce} harmonics do not correspond to resonance lines primarily because the long transmitter pulse prevented some of the short duration resonances from being observed. The calculated f_{ce} value is 4.96 kHz at this time, which is close to f_{ce} = 5.0 kHz at 2129 UT as expected. However, the f_{pe} value is difficult to determine on this particular Program 18 plasmagram because it is outside the

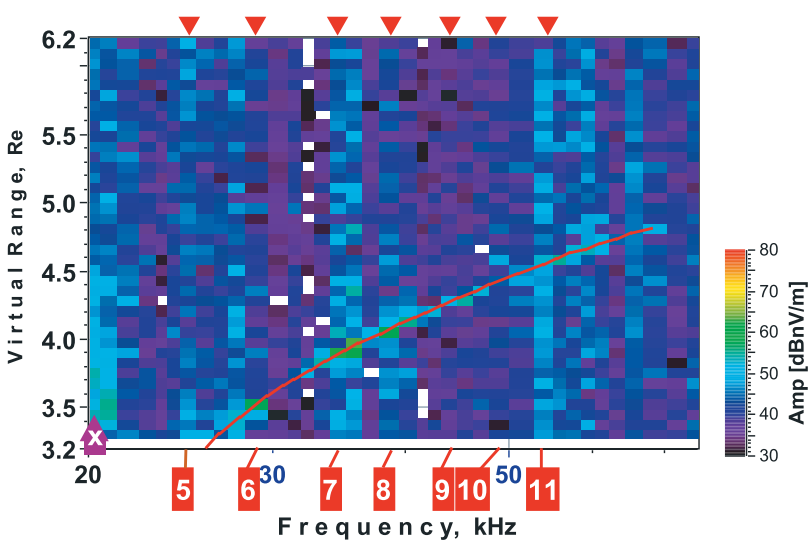

Figure 5. A plasmagram recorded with Program 18 at 2130 UT on 31 March 2001 presented with the similar format to that of Figure 2. The f_{ce} value is determined to be 4.96, and f_x value is set to its upper limit of 20.4 kHz. There is an X-mode trace extending from about 27.7 to 68.3 kHz.

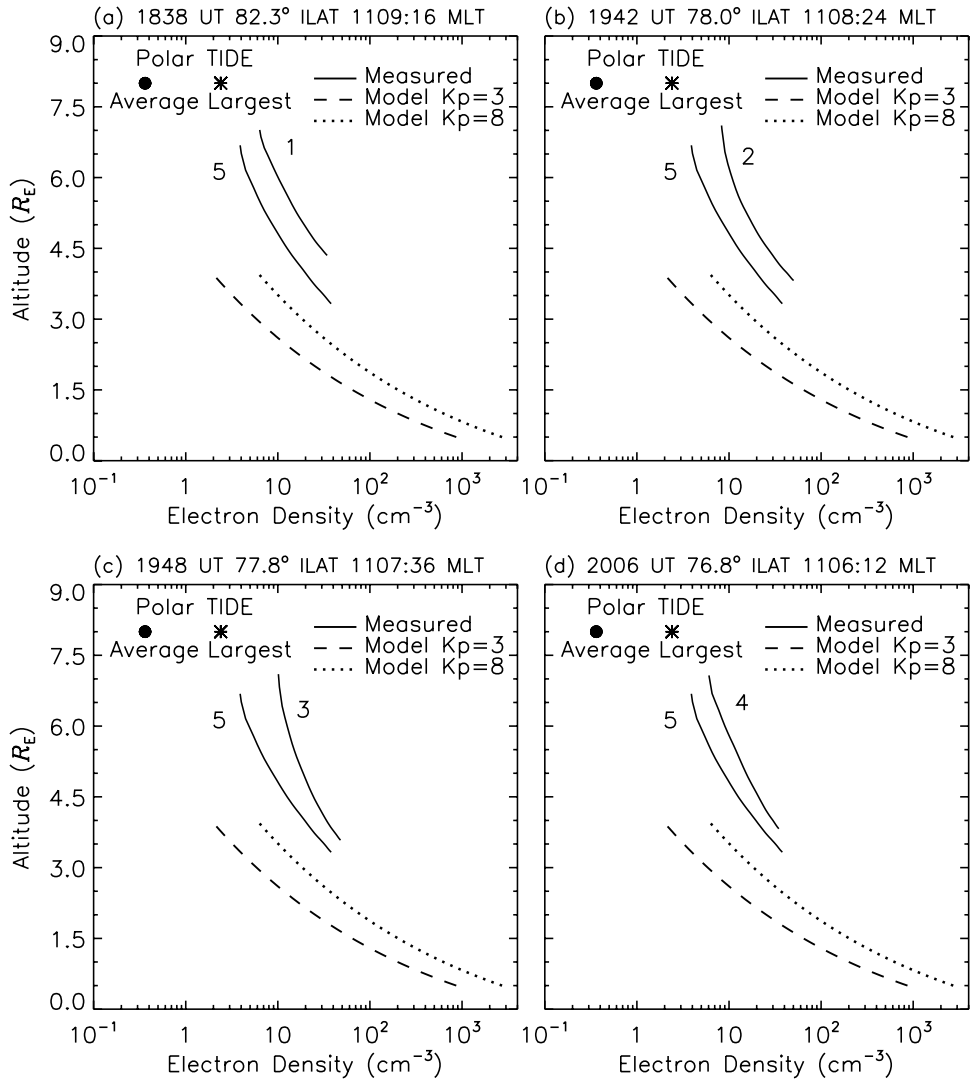

Figure 6. Measured field-aligned electron density distributions (solid lines) in the dayside polar cap derived from scaled traces on the plasmagrams recorded at the times listed in group 2 of Table 1. Density profiles 1–5 on panels (a)–(d) correspond to the plasmagram numbers. The dashed and dotted lines are density profiles from the empirical model of polar cap electron densities [*Nsumei et al.*, 2003] for Kp = 3 and Kp = 8, respectively. A dot and an asterisk represent average and largest total ion density, respectively, at 8 R_E altitude from the observations on thermal ion dynamics experiment (TIDE) aboard the POLAR satellite [*Su et al.*, 1998].

frequency range of the plasmagram. Its value can be in the range of 14.0–17.75 kHz from the variation trend of the X-mode trace on the plasmagram (see thin red line). *Osherovich et al.* [2007] have shown that the electron density along the IMAGE orbit over the polar cap was highly variable during the 31 March 2001 storm, implying that the f_{pe} value range of 14.0–17.75 kHz was possible. The value 14.0 kHz is close to f_{pe} = 12.0 kHz on the previous plasmagram (at 2129 UT). This will give f_x = 16.7 kHz, which is beyond the lowest frequency of the plasmagram, and we cannot get density profile inversion from the trace. Therefore we pick the upper limit of f_{pe} = 17.75 kHz and get an f_x value of 20.4 kHz, as indicated by a symbol X at the lower left corner of the plasmagram in Figure 5. We choose the upper limit to illustrate that the densities derived from this plasmagram are considerably lower than the densities derived from the other dayside plasmagrams, even if upper limit for f_{pe} value is used (see Figure 6).

[19] After f_{ce} and f_x are determined, we scale the trace and derive a field-aligned N_e profile (measurement 5 of group 2). The same procedure is applied to the other four dayside plasmagrams (listed as measurements 1–4 of group 2 in Table 1). Unlike the plasmagram at 2130 UT, the f_{pe} values on the other dayside plasmagrams can be fairly accurately determined with the aid of the f_{ce} and f_{pe} values on the adjacent Program 38 plasmagrams because the f_{pe} resonance is in the frequency range of those Program 18 plasmagrams and can be identified. The same procedure for estimating the uncertainty used for the nightside electron density profiles is also applied to the dayside density profiles. In Program 18, the frequency step below 50 kHz, where the resonances of

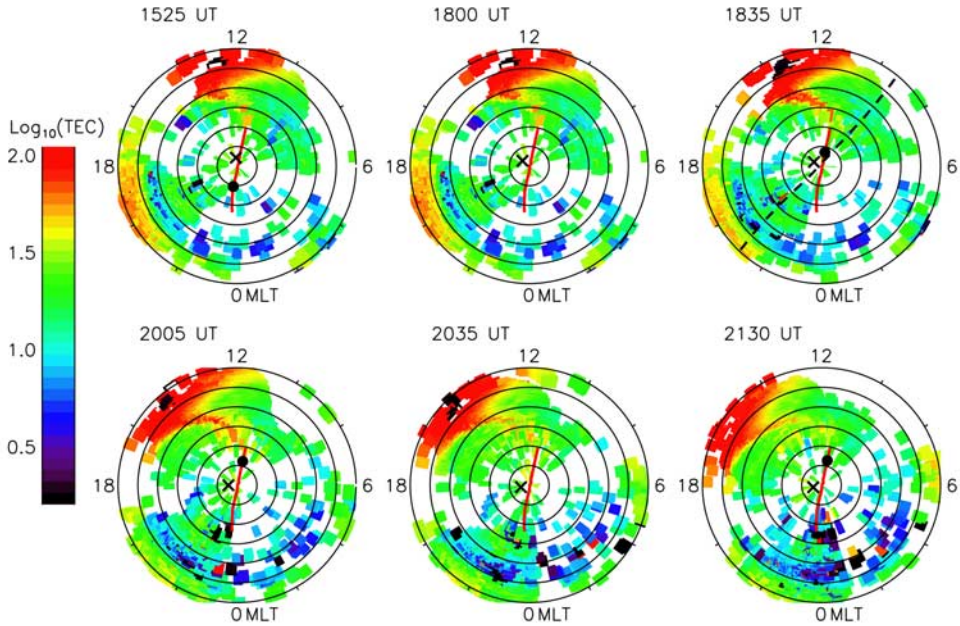

Figure 7. GPS TEC maps at 1525, 1800, 1835, 2005, 2035, and 2130 UT on 31 March 2001 are displayed in MLAT-MLT format. Latitude circles are at 10° interval. Overplotted red line is the footprint of the IMAGE orbit from 1400 to 2359 UT on 31 March 2001. On the TEC maps at 1525, 1835, 2005, and 2130 UT, the black dot on the IMAGE footprint indicates the location of the IMAGE at 1525, 1838, 2006, and 2130 UT, respectively. The black cross on each TEC map indicates the location of a Digisonde at Qaanaaq (85.7° MLAT). The dashed line on the TEC map at 1835 UT is the DMSP-F15 orbit from 1839 to 1912 UT on the same day.

the interest are detected, is 1.7 kHz. The uncertainty in the dayside density profiles is thus estimated to be up to 16%. It is hard to estimate the uncertainty for the density profile 5 since we are not able to carry out the density inversion with the lower limit of the f_{pe} = 14.0 kHz. However, we can calculate the uncertainty in the local electron density using the f_{pe} range of 14.0–17.75 kHz, which is determined to be ~60%.

[20] The field-aligned N_e profiles derived are displayed in Figures 6a–6d. The sequence (a)–(d) corresponds to measurements 1–4. The density profile 5, derived from the trace on the plasmagram shown in Figure 5, is repeatedly plotted in Figures 6a–6d. Unlike the other four dayside density profiles, profile 5 was estimated from an RPI measurement at the time when the TEC plume only existed at magnetic latitudes below 60°, as shown by the GPS TEC maps displayed in Figure 7. This is possibly the reason that the densities on profile 5 are lower than those on the other four profiles. We will discuss this issue in the next section. Note that in deriving density profile 5, an upper limit for the local f_{pe} is used. The actual densities on profile 5 may be even lower.

[21] On each panel of Figure 6 we also show, for reference, the average N_e from 3000 km to ~ 4 R_E altitude observed by *Nsumei et al.* [2003] for Kp = 3 (dashed line) and Kp = 8 (dotted line) using the IMAGE RPI sounding measurements. The average and the largest total ion densities (with an uncertainty ~11%) at 8 R_E altitude from the POLAR thermal ion dynamics experiment (TIDE) observed by *Su et al.* [1998] are also plotted, as a dot and an asterisk, respectively. It is seen that the densities are strongly enhanced up to 7 R_E altitude compared to the average density given by the IMAGE RPI and the POLAR TIDE observations, consistent with the electron density enhancements observed by *Osherovich et al.* [2001, 2007] and *Benson et al.* [2003, 2006] who showed that the polar cap densities were enhanced by a factor of about 2 compared to those before the magnetic storm. For example, the observed density at 4 R_E altitude ranges from ~20 to 41 cm^{-3}, about an order of magnitude larger than the average density at the same altitude from the observations of *Nsumei et al.* [2003], i.e., 1.9 and 5.9 cm^{-3} for Kp = 3 and Kp = 8, respectively. Note that Kp was equal to 8.3 at the times of the RPI measurements presented here. Furthermore, compared to the statistical density profiles, the measured density profiles have a smaller gradient; that is, the measured densities decrease significantly slower with altitude. Therefore the densities keep high values at higher altitudes: the presently observed in situ electron densities (at 7 R_E altitude) reach 10 cm^{-3}. An extrapolation of these density profiles to 8 R_E altitude gives electron densities of about 4–9 cm^{-3}, which are ~12–25 times and 2–3 times, respectively, higher than the average total ion density and the largest density value of 2.4 cm^{-3} measured by the POLAR TIDE at that altitude [*Su et al.*, 1998]. The derived polar cap densities for this magnetic storm period on the dayside and nightside were not in the database of *Nsumei et al.* [2003] and represent the most extreme polar cap densities ever observed by the RPI in our analyses so far. However, the spatially and temporally limited density measurements prevent us from determining the start time and the spatial distribution of the strong density enhance-

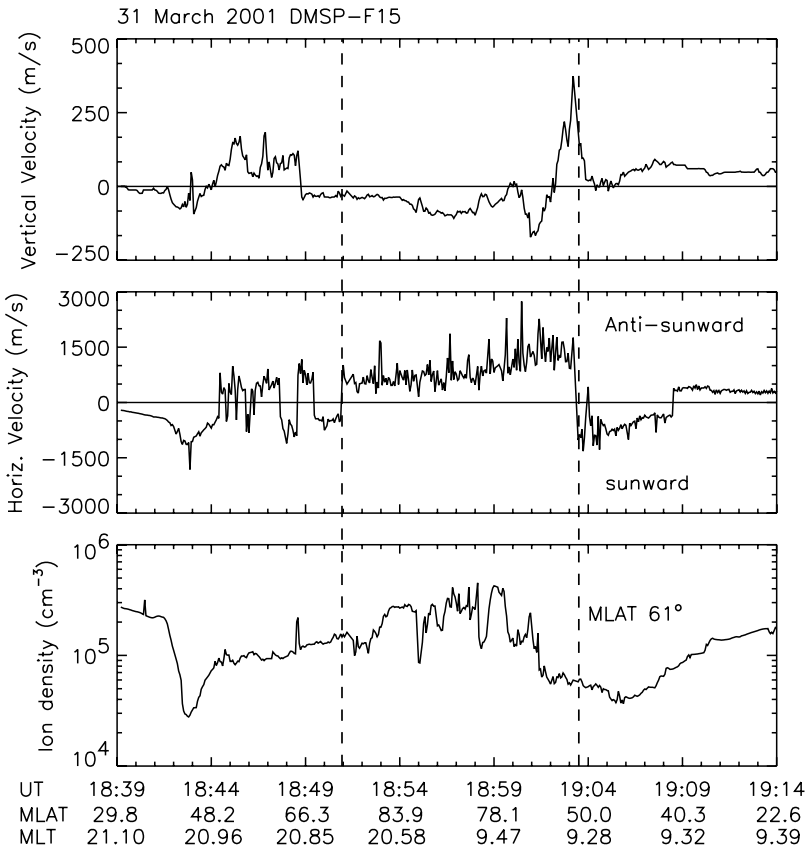

Figure 8. Variations of the vertical ion velocity (top panel), horizontal ion velocity (middle panel) and total ion density (bottom panel) along DMSP-F15 satellite orbit (at 840 km altitude) from 1839 to 1914 UT on 31 March 2001. The ionospheric convection velocity is anti-sunward in the polar cap (delineated by two dashed vertical lines). The satellite crossed morning-side convection reversal at 61° magnetic latitude at about 1903:30 UT (~0918:18 MLT).

ments in response to the extreme solar wind/IMF disturbances and examining the relative delay of the density enhancements to various processes that caused the density enhancements.

4. Plasma Plume Intrusion to High Latitudes

[22] As discussed in section 1, ionospheric and plasmaspheric plasma is redistributed during magnetic disturbances and a large flux of plasma from the midlatitude ionosphere (with a small contribution from the plasmaspheric drainage plume) may be transported to the polar latitudes. To explore the possible link between the strong density enhancements in the polar magnetosphere observed here (also by *Osherovich et al.* [2001, 2007] and *Benson et al.* [2003, 2006]) and the transport of the large flux of plasma from the midlatitude ionosphere, we present the TEC observations derived from data obtained from the global GPS network.

[23] The TEC derived from GPS receiver network is the number of electrons in a unit area column from 100 to 20,000 km (~3 R_E) above the Earth. The procedure to produce global TEC maps from data collected by the GPS receiver network is described by *Rideout and Coster* [2006]. *Coster et al.* [2003] have reported the GPS TEC observations made during the magnetic storm on 31 March 2001 and presented one TEC map (in geographic latitude and longitude format) at 1930 UT, demonstrating a TEC plume extending from midlatitude to high-latitude. In Figure 7, we display six selected GPS TEC maps in the Northern Hemisphere above 30° magnetic latitude in a format of MLAT-MLT. These six TEC maps were obtained at 1525, 1800, 1835, 2005, 2035, and 2130 UT, respectively. From the TEC maps and Table 1, we see that the nightside (group 1) measurements were made when there was no TEC plume intruding to high latitudes. They also show that the dayside (group 2) N_e profiles 1–4 were observed during the period when a TEC plume with TEC ≥~70 TEC units (1 TEC unit is 10^{16} electrons/m^2, column density) extended from about 50° MLAT and 1430 MLT to about 70° MLAT and 1200 MLT. The dayside density profile 5, however, was measured when the TEC plume had subsided below 60° MLAT. By examining a series of TEC maps on 31 March 2001, we see that a TEC plume existed from 1700 to 2200 UT. However, the strong TEC plume is seen extending to above 65° MLAT only within the interval from 1800 to 2035 UT (the dayside profiles 1–4 were measured within this interval, but the dayside profile 5 was not). The TEC plumes have been shown to occur along the common flux tubes with the plasmaspheric drainage plumes that intersect the dayside magnetopause [*Garcia et al.*, 2003; *Foster et al.*, 2004]. Note that the contribution to the TEC

plume is primarily from the ionospheric plasma. Therefore the TEC plume continuously carried a large flux of ionospheric plasma to the dayside auroral oval/cusp for about 2.5 hours (from 1800 to 2035 UT): the unit area flux inside the TEC plume reached 10^{15} electrons/m^2/s during the interval [*Coster et al.*, 2003]. After 2035 UT, the plasma flux transported to high latitudes became considerably smaller.

[24] As indicated previously, the cleft ion fountain effect can supply plasma to the polar magnetosphere. The large flux of ionospheric plasma intruding to high latitudes provides enhanced source population for the cleft ion fountain processes and thus may cause strongly enhanced plasma outflow (preferentially O^+ ions) flux along the field lines. As shown by previous observations [e.g., *Lockwood et al.*, 1985; *André*, 1990; *Dubouloz et al.*, 2001], the outflowing ionospheric ions are preferentially accelerated at altitudes below about 3–4 R_E. After exiting acceleration region and flowing further upward along the convecting flux tube, the velocities of the outflowing plasma decrease. Therefore, with the strongly enhanced outflow flux, the plasma density in the polar cap magnetosphere can be greatly enhanced if the convection in the polar cap is anti-sunward. The strongest electron density enhancements observed on the dayside polar magnetosphere, shown in Figure 6 as density profiles 1–4, are therefore likely due to the strongly enhanced cleft ion fountain effects. It should be noted that the cleft ion fountain effects take some time to transport the ionospheric plasma from its source region in the dayside cusp/auroral region to high altitudes in the polar cap. The actual delay time, which is dependent on the anti-sunward convection speed in the polar cap, can be several tens of minutes [e.g., *André et al.*, 1990; *Dubouloz et al.*, 2001; *Tu et al.*, 2004]. This means that the observed extremely high dayside N_e profiles were not instantly linked to the TEC plume at the times of the RPI observations but rather to the large flux of ionospheric plasma transported to the dayside aurora/cusp region several tens of minutes earlier.

[25] The densities on dayside profile 5 observed at 2130 UT are also enhanced compared to the average density profile for Kp = 8 (see Figure 6). This is true even if we take the lower limit of local f_{pe} value of 14.0 kHz (at 6.68 R_E altitude), which corresponds to an electron density of 2.43~cm^{-3} and is larger than the average density value of 0.66~cm^{-3} at the same altitude calculated using the model of *Nsumei et al.* [2003] for Kp = 8 assuming the model is applicable at that altitude. The enhancement, however, is not as strong as that of the densities on the dayside density profiles 1–4. As indicated previously, the TEC plume subsided to below 60° MLAT about 1 hour before the measurement of density profile 5. The dayside cusp/auroral region was at 61° MLAT or higher MLAT as will be shown by DMSP-F15 satellite data (see Figure 8 and associated discussion in section 5). Thus the ionospheric plasma flux transported to the dayside cusp/auroral region had been considerably weaker or even absent about 1 hour before the measurement of density profile 5. As a result of the weaker source population in the heating/acceleration region, the cleft ion fountain effects became weaker about 1 hour before the RPI measurement. This may explain the weaker electron density enhancement of profile 5. It is worth noting that the increase in the outflow ion flux occurs even without the ionospheric plasma being transported from lower latitudes to high latitudes. However, the cleft ion fountain effects are even more effective when the plasma plume from the lower latitudes provides the strongly enhanced source population in cusp/auroral region. Note that the convection in the polar cap was anti-sunward from 1415 to 2230 UT (see Figure 10), so the cleft ion fountain was in operation during this interval. Therefore the density enhancement on this profile relative to the model of Nsumei et al. was caused by the (less) enhanced cleft ion fountain. The causes of the nightside (group 1) electron density enhancements are more complicated because they were observed around the time when the IMF B_z changed from northward to southward. We will discuss the causes of the density enhancements on nightside electron when describing the observations of the ionospheric velocity and density in the following section.

5. Ionospheric Plasma Velocity and Density

[26] It has been shown in Figure 1 that the IMF B_z was strongly negative at times of group 2 measurements of the IMAGE RPI and had been strongly negative for over 5 hours before the measurements. The convection at high latitudes was expected to be anti-sunward in the polar cap for this interval covering the RPI measurements. To see if this is the case, we present in Figure 8 variations of the ion vertical velocity (top panel), horizontal velocity (middle panel), and the total ion density (bottom panel) along the DMSP-F15 satellite orbit (at 840 km altitude) from 1839 to 1914 UT on 31 March 2001. The horizontal velocities do show anti-sunward convection between 61° MLAT on the morning side (MLT = 9.29) and 68° MLAT on the evening side (MLT = 20.84). The dayside auroral oval magnetic latitude was close to 61° MLAT because of the convection reversal at this latitude and because of the enhanced upward vertical velocities in a narrow latitude region poleward of it (top panel of Figure 8). The observed enhanced upward velocities are the expected ionospheric upflows in the region around the poleward boundary of the auroral oval [e.g., *Lockwood et al.*, 1985; *Tsunoda et al.*, 1989; *Dubouloz et al.*, 2001]. The cusp was thus located at 61° or higher MLAT because the cusp should be on the open magnetic field lines, poleward of the dayside auroral oval.

[27] It is interesting to note that the polar cap total ion (primarily O^+ ions) density in the topside ionosphere was at the level of the density at latitudes below about 30° (see bottom panel of Figure 8). The measurements from the Digisonde in the central polar cap also show increased ionospheric density. Figure 9 displays the electron plasma frequency variations with altitude and universal time derived from the measurements made by the Digisonde at Qaanaaq (geographic lat./lon. 77.5°/290.8°; magnetic lat./lon. 85.7°/33.1°). The Digisonde measures an electron density profile (note that $N_e \propto f_{pe}^2$) up to the F-region peak altitude every 5–15 min, and the densities above the F-peak altitude are extrapolated using an α-Chapman distribution with a constant scale height that is derived from the measured bottomside density profile [*Reinisch et al.*, 2005]. Figure 9 shows that the ionospheric density at all altitudes started to increase at about 1600 UT (and a strong density enhancement was observed in the period of 1715–2130 UT, roughly coincident with the period when a TEC

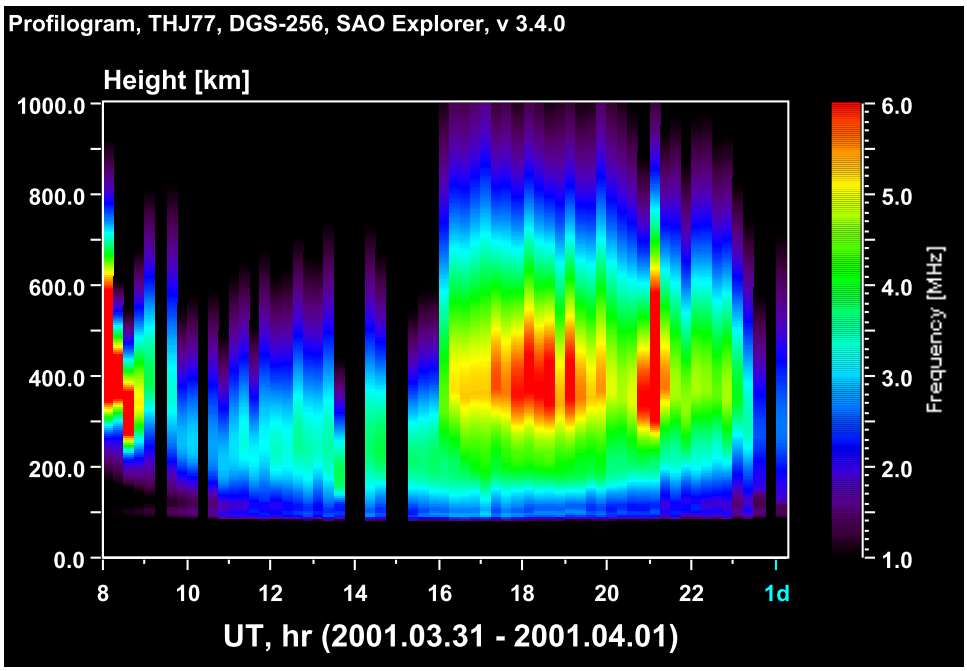

Figure 9. Electron plasma frequency variations with altitude and universal time measured by the Digisonde in the polar cap (at Qaanaaq, geographic lat./lon. 77.5°/290.8°; magnetic lat./lon. 85.7°/33.1°) from 0800 to 2400 UT on 31 March 2001.

plume existed). Thus such a high ionospheric density might be the consequence of the plasma plume intruding to the high latitudes [e.g., *Foster et al.*, 2005; *Sojka et al.*, 2006]. This interesting issue will be the topic of our future study. We have a limited time period of DMSP-F15 observations that show the anti-sunward convection in the polar cap because the satellite and other DMSP satellites did not provide reliable plasma velocity measure-

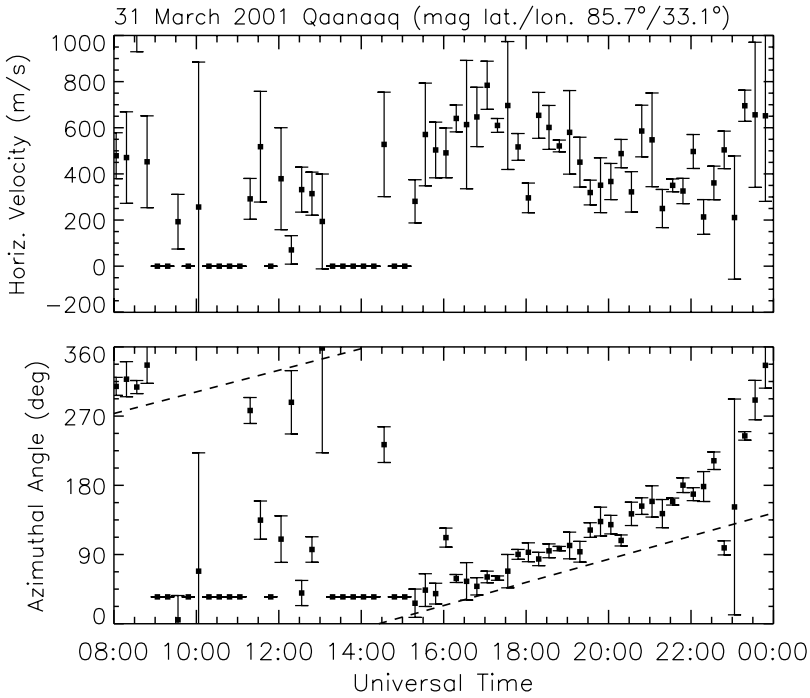

Figure 10. Digisonde observations of the horizontal plasma drift velocity at F-layer altitudes in the polar cap at Qaanaaq from 0800 to 2400 UT on 31 March 2001. The upper panel shows the horizontal drift velocity magnitude while the lower panel displays the azimuthal angle from the local magnetic north of the velocity vectors. The dashed lines represent the anti-sunward direction. The error bars represent standard deviations.

ments in the polar cap for other periods on this day. In order to get further information about the polar cap convection, we examined the Digisonde observations of the electron drift velocities [*Reinisch et al.*, 1987, 2005] at Qaanaaq in the central polar cap (magnetic latitude 85.7°). Figure 10 displays the variations of horizontal velocities in the F region from 0800 to 2400 UT on 31 March 2001. The top panel shows the magnitude of the horizontal velocity while the bottom panel shows the azimuthal angle of the velocity vectors with respect to local magnetic north. The dashed lines indicate anti-sunward direction. It is seen that the horizontal drift velocities in the F-layer were about 600–800 m/s primarily in the anti-sunward direction from about 1415 to 1900 UT. Since then, the velocities remained anti-sunward with velocity magnitude of ~400 m/s until about 2200 UT. This period of anti-sunward polar cap convection covers the RPI dayside measurements and nightside measurements after 1500 UT.

[28] Figure 10 also shows that prior to 1415 UT, the velocities measured by the Digisonde were not systematically anti-sunward or sunward, implying a complicated polar cap convection pattern during the period of IMF B_z northward and around the IMF re-orientation. The nightside density profiles (group 1) measured by the IMAGE RPI before 1443 UT therefore might not be related to the cleft ion fountain that requires anti-sunward convection to transport outflowing ionospheric plasma from its source region in the dayside auroral/cusp region to the polar cap because the anti-sunward transport takes a certain amount of time. The density enhancements on the nightside profiles measured before 1443 UT might be due to the increased local ion outflows in the polar cap since the polar cap auroral processes during northward IMF B_z can drive upward ion flows in the polar cap. With the current data set, however, we cannot definitely determine the causes of the density enhancements observed at those times. Nevertheless, the density enhancements observed about 1 hour later (at 1513 and 1525 UT) were most likely caused by the cleft ion fountain effects because the convection had turned to anti-sunward about 1 hour before these two measurements. Note that during the period of anti-sunward convection driven by the southward IMF B_z there should be no auroral activities in the polar cap to drive upward ion flows locally.

6. Discussion and Summary

[29] We have presented the IMAGE RPI measurements of the field-aligned electron density distributions from an IMAGE polar cap pass from nightside to dayside during the 31 March 2001 magnetic storm. The RPI observed density enhancements on both the nightside and dayside in the polar cap. The nightside measurements were made at altitudes below about 5 R_E while the observed dayside density profiles extended to ~7 R_E altitude. Density observations at such high altitudes and even higher altitudes have been made previously using in situ measurements [e.g., *Marklund et al.*, 1990; *Laakso et al.*, 2002; *Osherovich et al.*, 2001, 2007; *Benson et al.*, 2003, 2006]. Instantaneously measured field-aligned density profiles in the polar cap have also been reported previously for the altitudes below about 4 R_E [*Nsumei et al.*, 2003; *Tu et al.*, 2005b]. However, the instantaneously measured field-aligned density profiles up to 7 R_E altitude are, for the first time, presented in this study. It is shown that the N_e profiles were strongly enhanced at least up to 7 R_E altitude during the storm on 31 March 2001. The density at 7 R_E reached about 10 cm^{-3}, an unusually high value at that altitude because it is even higher than the average density observed previously at 4 R_E altitude ($\leq$ 6 cm^{-3}). Compared to the average density profiles obtained from IMAGE RPI measurements in the work of *Nsumei et al.* [2003], the presently measured density profiles show large density enhancements at all altitudes. During the storm, a strong ionospheric plume, extending from midlatitude ionosphere across the dayside auroral/cusp to high latitudes, existed from 1800 to 2035 UT. The plume continuously provided an enhanced source population for about 2.5 hours for the potential outflow of the large flux of ionospheric plasma along magnetic field lines. The high-latitude convection as shown by the DMSP-F15 observations was anti-sunward in the polar cap and remained anti-sunward from 1415 to 2200 UT as revealed by Digisonde F-region electron drift measurements in the central polar cap.

[30] The cleft ion fountain operates when the polar cap convection is anti-sunward. During geomagnetic disturbances, the cleft ion fountain effect may be strengthened by increased energy deposit to the high-latitude ionosphere and thus result in enhanced polar cap densities at high altitudes [e.g., *Tu et al.*, 2004]. The ionospheric plasma plume may cause even more greatly enhanced source population for the cleft ion fountain effect. This is perhaps the cause of the strongest density enhancements shown by the density profiles 1–4 observed on the dayside (Figure 6). Although there are no direct observations of the ionospheric outflows during the period of interest, strong ionospheric ion outflows have been observed by the Cluster satellites during the main phase of the storm from 0800 to 0930 UT [*Korth et al.*, 2004]. Within the period of the second decrease of the Dst driven by strongly negative IMF B_z which lasted for more than 5 hours (see Figure 1), ionospheric ion outflows are also expected to occur. The present observations suggest that the most strongly enhanced density extending to high altitudes in the polar cap is likely caused by the greatly enhanced cleft ion fountain that supplies plasma into the polar cap magnetosphere with the enhanced source population in the cusp/auroral region.

[31] The TEC plume intruding to the polar cap also includes a contribution from the plasmaspheric plasma, which is stripped away from the outer edge of the plasmasphere. The stripped plasmaspheric plasma is transported to the dayside magnetopause and may directly account for part of the density enhancements in the polar magnetosphere. Nevertheless, the major contribution to the TEC plume is from the ionosphere [*Foster et al.*, 2004; *Huang et al.*, 2005], which provided greatly strengthened source population for the cleft ion fountain. Therefore the cleft ion fountain that transports outflowing ionospheric plasma to the polar magnetosphere may be the primary source of the density enhancements, particularly for the dayside density enhancements. The present observations, however, do not allow us to examine in detail the possible link between the plasma plume and the strongest density enhancements (for example, the time delay between the arrival of the TEC plume to the cusp/auroral region and the polar magneto-

spheric density enhancements), as this requires information about the global high-latitude convection pattern and history (which may be obtained by the SuperDan radar network). In addition, one needs information about the spatial and temporal variations of the heating/acceleration processes in the dayside cusp/aurora region in order to evaluate the plasma transport. This information is not yet available. The present observations can provide constrains to the simulations that explore the spatial and temporal variations of those heating/acceleration processes.

[32] It has been noted in Figure 8 that the topside ionosphere density in the polar cap was increased during the period when the TEC plume was observed to intrude across the dayside auroral/cusp to the polar cap. This increased ionospheric ion (primarily O^+) density can also induce increased ion outflows locally in the polar cap and thus may contribute to the density enhancements at high altitudes. However, the DMSP-F15 satellite observed downward O^+ ion vertical velocity in the polar cap for the period from 1851 to 1903 UT. Therefore the outflows of O^+ from the polar cap may be ruled out for the dayside measurements. We do not have enough information about the H^+ outflows (polar wind), so we cannot assess the relative importance of the enhanced cleft ion fountain effects and the locally enhanced polar wind in causing the observed polar magnetosphere density enhancements. Nevertheless, it is reasonable to suggest that the greatly enhanced cleft ion fountain is responsible for the density enhancements, at least for the strongest enhancements on the dayside (profiles 1–4 in Figure 6) because of the considerably weaker density enhancement (profile 5 in Figure 6) when the plasma plume subsided to below 60° MLAT. When the plasma plume subsided, significantly less (even absent) flux of ionospheric plasma is transported to the dayside auroral/cusp for the ion outflows, resulting in a weaker cleft ion fountain and thus causing weaker density enhancement at high altitudes in the polar cap (compare profile 5 to profiles 1–4 in Figure 6). Other evidence that supports this conjecture is that the outflow flux of ionospheric ions is increased primarily due to an increase in the O^+ outflow flux [e.g., *Moore et al.*, 1999]. Without locally observed O^+ outflow in the polar cap, the cleft ion fountain is thus the most likely mechanism for the dayside density enhancements observed in the polar magnetosphere.

[33] The present IMAGE RPI observations display xtreme electron density enhancements along magnetic field lines in the polar cap extending to 7 R_E altitude. The enhanced cleft ion fountain effects are believed to be responsible for the observed density enhancements although some of the nightside density enhancements may be caused by the increase of the ion outflows locally in the polar cap. The strongest density enhancements observed on the dayside are also likely associated with the plasma plume transporting primarily ionospheric plasma from lower latitudes to the dayside auroral/cusp region that further strengthened the cleft ion fountain. The present study and the works of *Osherovich et al.* [2001, 2007] and *Benson et al.* [2003, 2006] show that during magnetic storms the plasma density is globally redistributed not only in the ionosphere and plasmasphere, as is already well known, but also in the polar magnetosphere.

[34] **Acknowledgments.** This work was supported by NASA under subcontract 83822 from the Southwest Research Institute, by NSF grant NSF-ATM 0518227 to the University of Massachusetts Lowell, and by Air Force award F19628-C-0092. The World Data Center for Geomagnetism (WDC-C2) at Kyoto University, Japan, provided the Dst data. Kp indices were provided by the National Geophysical Data Center. The ACE solar wind and IMF data are obtained from the CDAWeb system (http://cdaweb.gsfc.nasa.gov/). We gratefully acknowledge the Center for Space Sciences at the University of Texas at Dallas and the U.S. Air Force for providing the DMSP thermal plasma data.

[35] Wolfgang Baumjohann thanks Kristian Schlegel and another reviewer for their assistance in evaluating this paper.

References

André, M., G. B. Crew, W. K. Peterson, A. M. Persoon, C. J. Pollock, and M. J. Engebretson (1990), Ion heating by broadband low-frequency waves in the cusp/cleft, *J. Geophys. Res.*, *95*, 20,809–20,823.

Benson, R. F., V. A. Osherovich, J. Fainberg, and B. W. Reinisch (2003), Classification of IMAGE/RPI-stimulated plasma resonances for the accurate determination of magnetospheric electron density and magnetic field values, *J. Geophys. Res.*, *108*(A5), 1207, doi:10.1029/2002JA009589.

Benson, R. F., V. A. Osherovich, J. Fainberg, J. L. Green, S. A. Boardsen, L. N. Garcia, N. Tsyganenko, and B. W. Reinisch (2006), RPI/IMAGE plasma and magnetic signatures of solar-wind/magnetosphere interactions, *Eos Trans. AGU*, *87*(36), Jt. Assem. Suppl., Abstract SM42A-05.

Buonsanto, M. J. (1999), Ionospheric storms – A review, *Space Sci. Rev.*, *88*, 563–601.

Burch, J. L., et al. (2001), Views of Earth's magnetosphere with the IMAGE satellite, *Science*, *291*(5504), 619–624.

Chappell, C. R., T. E. Moore, and J. H. Waite Jr. (1987), The ionosphere as a fully adequate source of plasma for the Earth's magnetosphere, *J. Geophys. Res.*, *92*, 5896–5910.

Chappell, C. R., B. L. Giles, T. E. Moore, D. C. Delcourt, P. D. Craven, and M. O. Chandler (2000), The adequacy of ionospheric source in supplying magnetosphere plasma, *J. Atmos. Sol. Terr. Phys.*, *62*, 421–436.

Coster, A. J., J. Foster, and P. Erickson (2003), Monitoring the ionosphere with GPS: Space weather, *GPS World*, *14*(5), 40–45.

Dubouloz, N., M. Bouhram, C. Senior, D. Delcourt, M. Malingre, and J.-A. Sauvaud (2001), Spatial structure of the cusp/cleft ion fountain: A case study using a magnetic conjugacy between Interball AP and a pair of SuperDARN radars, *J. Geophys. Res.*, *106*, 261–274.

Evans, J. V. (1973), The causes of storm-time increases of the F-layer at mid-latitudes, *J. Atmos. Sol. Terr. Phys.*, *35*, 593–616.

Foster, J. C. (1993), Storm time plasma transport at middle and high latitudes, *J. Geophys. Res.*, *98*, 1675–1689.

Foster, J. C., P. J. Erickson, A. J. Coster, J. Goldstein, and F. J. Rich (2002), Ionospheric signatures of plasmaspheric tails, *Geophys. Res. Lett.*, *29*(13), 1263, doi:10.1029/2002GL015067.

Foster, J. C., A. J. Coster, P. J. Erickson, F. J. Rich, and B. R. Sandel (2004), Storm-time observations of the flux of plasmaspheric ions to the dayside cusp/magnetopause, *Geophys. Res. Lett.*, *31*(8), L08809, doi:10.1029/2004GL020082.

Foster, J. C., et al. (2005), Multiradar observations of the polar tongue of ionization, *J. Geophys. Res.*, *110*(A9), A09S31, doi:10.1029/2004JA010928.

Fung, S. F., and J. L. Green (2005), Modeling of field-aligned radio echoes in the plasmasphere, *J. Geophys. Res.*, *110*(A1), A01210, doi:10.1029/2004JA010658.

Fung, S. F., R. F. Benson, D. L. Carpenter, J. L. Green, V. Jayanti, I. A. Galkin, and B. W. Reinisch (2003), Guided echoes in the magnetosphere: Observations by radio plasma imager on IMAGE, *Geophys. Res. Lett.*, *30*(11), 1589, doi:10.1029/2002GL016531.

Galkin, I., B. W. Reinisch, G. Grinstein, G. Khmyrov, A. Kozlov, X. Huang, and S. Fung (2004), Automated exploration of the radio plasma imager data, *J. Geophys. Res.*, *109*(A12), A12210, doi:10.1029/2004JA010439.

Garcia, L. N., S. F. Fung, J. L. Green, S. A. Boardsen, B. R. Sandel, and B. W. Reinisch (2003), Observations of the latitudinal structure of plasmaspheric convection plumes by IMAGE-RPI and EUV, *J. Geophys. Res.*, *108*(A8), 1321, doi:10.1029/2002JA009496.

Hoegy, W. R., and R. F. Benson (1988), DE/ISIS conjunction comparisons of high-latitude electron density features, *J. Geophys. Res.*, *93*, 5947–5954.

Horwitz, J. L. (1984), Features of ion trajectories in the polar magnetosphere, *Geophys. Res. Lett.*, *11*, 1111–1114.

Horwitz, J. L., and T. E. Moore (1997), Four contemporary issues concerning ionospheric plasma flow to the magnetosphere, *Space Sci. Rev.*, *80*, 49–76.

Huang, X., B. W. Reinisch, P. Song, J. L. Green, and D. L. Gallagher (2004), Developing an empirical density model of the plasmasphere using IMAGE/RPI observations, *Adv. Space Res.*, *33*, 829–832.

Huang, C. S., J. C. Foster, L. P. Goncharenko, P. J. Erickson, W. Rideout, and A. J. Coster (2005), A strong positive phase of ionospheric storms observed by the Millstone Hill incoherent scatter radar and global GPS network, *J. Geophys. Res.*, *110*(A6), A06303, doi:10.1029/2004JA010865.

Korth, A., et al. (2004), Ion injections at auroral latitude during the March 31, 2001 magnetic storm observed by Cluster, *Geophys. Res. Lett.*, *31*(20), L20806, doi:10.1029/2004GL020356.

Laakso, H., R. Pfaff, and P. Janhunen (2002), Polar observations of electron density distribution in the Earth's magnetosphere: 2. Density profiles, *Ann. Geophys.*, *20*, 1725–1735.

Lockwood, M., M. O. Chandler, J. L. Horwitz, J. H. Waite Jr., T. E. Moore, and C. R. Chappell (1985), The cleft ion fountain, *J. Geophys. Res.*, *90*, 9736–9748.

Marklund, G. T., L. G. Blomberg, C.-G. Falthammar, R. E. Erlandson, and T. A. Potemra (1990), Signatures of the high-altitude polar cusp and dayside auroral regions as seen by the Viking electric field experiment, *J. Geophys. Res.*, *95*, 5767–5780.

Moore, T. E., and D. C. Delcourt (1995), The geopause, *Rev. Geophys.*, *33*, 175–209.

Moore, T. E., R. Lundin, D. Alcayde, M. André, S. B. Ganguli, M. Temerin, and A. Yau (1999), Source processes in the high-latitude ionosphere, in *Magnetospheric Plasma Sources and Losses*, edited by B. Hultqvist, M. Øieroset, G. Paschmann, and R. Treumann, pp. 7–84, Springer, New York.

Muldrew, D. B. (1972), Electrostatic resonances associated with the maximum frequencies of cyclotron-harmonic waves, *J. Geophys. Res.*, *77*, 1794–1801.

Nsumei, P. A., X. Huang, B. W. Reinisch, P. Song, V. M. Vasyliūnas, J. L. Green, S. F. Fung, R. F. Benson, and D. L. Gallagher (2003), Electron density distribution over the northern polar region deduced from IMAGE/radio plasma imager sounding, *J. Geophys. Res.*, *108*(A2), 1078, doi:10.1029/2002JA009616.

Osherovich, V.A., R.F. Benson, J. Fainberg, and B.W. Reinisch (2001), Increased magnetospheric f_{pe}/f_{ce} values in response to magnetic-cloud enhancements of the solar-wind quasi-invariant on March 31 2001, *Eos Trans. AGU*, *82*(47), Fall Meet. Suppl., Abstract SM31B-0758.

Osherovich, V. A., R. F. Benson, and J. Fainberg (2005), Electromagnetic bounded states and challenges of plasma spectroscopy, *IEEE Trans. Plasma Sci.*, *33*, 599–608.

Osherovich, V. A., R. F. Benson, J. Fainberg, J. L. Green, L. Garcia, S. Boardsen, N. Tsyganenko, and B. W. Reinisch (2007), Enhanced high-altitude polar-cap plasma and magnetic-field values in response to interplanetary magnetic cloud that caused the great storm of 31 March 2001: A case study for a new magnetospheric index, *J. Geophys. Res.*, in press.

Pryse, S. E., R. W. Sims, J. Moen, L. Kersley, D. Lorentzen, and W. F. Denig (2004), Evidence for solar production as a source of polar cap plasma, *Ann. Geophys.*, *22*(4), 1093–1102.

Reinisch, B. W., J. Buchau, and E. J. Weber (1987), Digital ionosonde observations of the polar cap F region convection, *Phys. Scr.*, *36*, 372–377.

Reinisch, B. W., et al. (2000), The radio plasma imager investigation on the IMAGE spacecraft, *Space Sci. Rev.*, *91*, 319–359.

Reinisch, B. W., X. Huang, P. Song, G. S. Sales, S. F. Fung, J. L. Green, D. L. Gallagher, and V. M. Vasyliūnas (2001), Plasma density distribution along the magnetospheric field: RPI observations from IMAGE, *Geophys. Res. Lett.*, *28*, 4521–4524.

Reinisch, B. W., X. Huang, P. Song, J. L. Green, S. F. Fung, V. M. Vasyliūnas, D. L. Gallagher, and B. R. Sandel (2004), Plasmaspheric mass loss and refilling as a result of a magnetic storm, *J. Geophys. Res.*, *109*(A1), A01202, doi:10.1029/2003JA009948.

Reinisch, B. W., X. Huang, I. A. Galkin, V. Paznukhov, and A. Kozlov (2005), Recent advances in real-time analysis of ionograms and ionospheric drift measurements with Digisondes, *J. Atmos. Sol. Terr. Phys.*, *67*, 1054–1062.

Rideout, W., and A. Coster (2006), Automated GPS processing for global total electron content data, *GPS Solut.*, *10*, 219–228.

Rodger, A. S., M. Pinnock, J. R. Dudeney, K. B. Baker, and R. A. Greenwald (1994), A new mechanism for polar patch formation, *J. Geophys. Res.*, *99*, 6425–6436.

Schunk, R. W. (2000), Theoretical developments on the causes of ionospheric outflow, *J. Atmos. Sol. Terr. Phys.*, *62*, 399–420.

Schunk, R. W., and J. J. Sojka (1997), Global ionosphere–polar wind system during changing magnetic activity, *J. Geophys. Res.*, *102*, 11,625–11,652.

Sojka, J. J., C. Smithtro, and R. W. Schunk (2006), Recent developments in ionosphere–thermosphere modeling with an emphasis on solar-variability, *Adv. Space Res.*, *37*, 369–379.

Song, P., B. W. Reinisch, X. Huang, and J. L. Green (2004), Magnetospheric active wave measurements, *COSPAR Colloq. Ser.*, *16*, 235–246.

Stix, T. H. (1962), *The Theory of Plasma Waves*, 283 pp., McGraw-Hill, New York.

Su, Y.-J., J. L. Horwitz, T. E. Moore, B. L. Giles, M. O. Chandler, P. D. Craven, M. Hirahara, and C. J. Pollock (1998), Polar wind survey with the thermal ion dynamics experiment/plasma source instrument suite aboard POLAR, *J. Geophys. Res.*, *103*, 29,305–29,337.

Tanaka, T. (1979), The worldwide distribution of positive ionospheric storms, *J. Atmos. Terr. Phys.*, *41*, 103–110.

Tsunoda, R. T., R. C. Livingston, J. F. Vickrey, R. A. Heelis, W. B. Hanson, F. J. Rich, and P. F. Bythrow (1989), Dayside observations of thermal-ion upwelling at 800-km altitude: An ionospheric signature of the cleft ion fountain, *J. Geophys. Res.*, *94*, 15,277–15,290.

Tsurutani, B., et al. (2004), Global dayside ionospheric uplift and enhancement associated with interplanetary electric fields, *J. Geophys. Res.*, *109*(A8), A08302, doi:10.1029/2003JA010342.

Tsyganenko, N. A. (2002), A model of magnetosphere with a dawn–dusk asymmetry: 2. Parameterization and fitting to observations, *J. Geophys. Res.*, *107*(A7), 1176, doi:10.1029/2001JA000220.

Tu, J.-N., J. L. Horwitz, P. A. Nsumei, P. Song, X.-Q. Huang, and B. W. Reinisch (2004), Simulation of polar cap field-aligned electron density profiles measured with the IMAGE radio plasma imager, *J. Geophys. Res.*, *109*(A7), A07206, doi:10.1029/2003JA010310.

Tu, J.-N., J. L. Horwitz, and T. E. Moore (2005a), Simulating the cleft ion fountain at polar perigee altitudes, *J. Atmos. Sol. Terr. Phys.*, *67*, 465–477.

Tu, J.-N., P. Song, B. W. Reinisch, X. Huang, J. L. Green, H. U. Frey, and P. H. Reiff (2005b), Electron density images of the middle- and high-latitude magnetosphere in response to the solar wind, *J. Geophys. Res.*, *110*(A12), A12210, doi:10.1029/2005JA011328.

Warren, E. S. (1969), The topside ionosphere during geomagnetic storms, *Proc. IEEE*, *57*, 1029–1036.

Whitteker, J. H., L. H. Brace, E. J. Maier, J. R. Burrows, W. H. Dodson, and J. D. Winningham (1976), A snapshot of the polar ionosphere, *Planet. Space Sci.*, *24*, 25–28.

Zeng, W., J. L. Horwitz, P. D. Craven, F. J. Rich, and T. E. Moore (2004), The O^+ density trough at 5000 km altitude in the polar cap, *J. Geophys. Res.*, *109*(A9), A03220, doi:10.1029/2003JA010210.

R. F. Benson, NASA Goddard Space Flight Center, Code 612.2, Bldg 21, Greenbelt, MD 20771, USA. (robert.f.benson@nasa.gov)

A. J. Coster, Atmospheric Sciences, MIT Haystack Observatory, Westford, MA 01886, USA. (ajc@haystack.mit.edu)

M. Dhar, B. W. Reinisch, P. Song, and J.-N. Tu, Center for Atmospheric Research, University of Massachusetts Lowell, 600 Suffolk Street, Lowell, MA 01854, USA. (jiannan_tu@uml.edu)

J. L. Green, NASA Goddard Space Flight Center, Code 605, Bldg 26, Greenbelt, MD 20771, USA. (james.green@nasa.gov)